

Anomalous Criticality of Absorbing State Transition toward Jamming

He-Da Wang,^{1,2,3} Bo Wang,^{1,2,3} Qun-Li Lei,^{1,2,3,4,*} and Yu-Qiang Ma^{1,2,3,4,†}

¹*National Laboratory of Solid State Microstructures, Nanjing University, Nanjing 210093, China*

²*Collaborative Innovation Center of Advanced Microstructures and*

School of Physics, Nanjing University, Nanjing 210093, China

³*Jiangsu Physical Science Research Center, Nanjing 210093, China*

⁴*Hefei National Laboratory, Shanghai 201315, China*

(Dated: March 18, 2026)

Abstract: Jamming transition is traditionally regarded as a geometric transition governed by static contact networks. Recently, dynamic phase transitions of athermal particles under periodic shearing provide a new lens on this problem, leading to a conjecture that jamming transition corresponds to an absorbing-state transition within the Manna (conserved directed percolation) universality class. Here, by re-examining biased random organization models, minimal models for particles under periodic shearing that the conjecture is based on, we uncover several criticality anomalies at high density at odds with the Manna universality class. In three-dimensional monodisperse systems, we find crystallization disrupts the absorbing transition, while in dense binary mixtures, a distinct transition from absorbing to active-glass state emerges, signifying a new dynamic universality class. Close to the jamming point, the quenched heterogeneity in the contact network of binary systems smears the dynamic criticality via Griffiths effects and drives the system toward heterogeneous directed percolation. For close-packed crystal structures, Griffiths effect is absent. However, the dynamic criticality still deviates from the Manna model. These phenomena are explained by a field theory with fractional time dynamics that links jamming, disorder and dynamic criticality.

POPULAR SUMMARY

Jamming transition, when materials like sand or foam suddenly become rigid, is traditionally viewed as a geometric packing problem. Recent ideas suggest it's also tied to a criticality of dynamic processes, like how crowded particles stop moving under repeated shaking or shearing. This work puts these ideas to the test and reveals a more complex and fascinating story: at intermediate high density, a new universality class of dynamic transition from absorbing to active-glass state emerges, while near the jamming point, heterogeneity induces Griffiths effects smearing out the dynamic critical point. Our work reveals complicated interplay between static and dynamic phase transitions and sheds light on the dynamic criticality of high-dimensional disordered systems, like learning processes of artificial neural networks.

INTRODUCTION

The jamming transition, a transition from a mechanically soft state to a rigid state, widely exists in soft matter systems [1–4]. The static packing of spheres provides a natural route to study the jamming transition, in which the random close packing (RCP) state is introduced to describe the most compact state that spheres can be arranged in a random way [5–7]. Although the RCP state can be protocol-dependent [8, 9], it is still widely regarded as a signature of the jamming transition [10–17].

Another path to tackle the jamming problem is from the dynamic side. It was first found that when dilute suspended colloidal particles are subjected to pe-

riodic shearing, a reversible to irreversible transition, or an absorbing state transition, can occur upon increasing the shearing amplitude [18–20]. As system density increases, the critical shearing amplitude becomes smaller, making the reversible to irreversible transition coincide with the jamming transition [4, 20–30]. Nevertheless, directly studying the criticality of such a dynamic transition at high density is challenging, due to the divergent relaxation time and long-range correlation near the jamming point [20, 23–25]. Theoretically, the many-body dynamics of particles under periodic shearing can be well captured by a minimal model, i.e., the random organization (RO) model [19, 31, 32]. Recent works have demonstrated that the biased random organization (BRO) model, a more realistic version of the RO model in which the displacements of particles are not fully random but repulsive, can generate the RCP state at the critical point of the absorbing transition when the displacement size (corresponding to shearing amplitude) vanishes ($\varepsilon \rightarrow 0$) in dimensions $d=1$ to 5 [33–35]. The RO/BRO model in the dilute regime has been proven to belong to the Manna universality class, or conserved directed percolation (CDP) [22, 36–39]. In Ref. [33, 34, 40], it was suggested that the BRO model also resides in the Manna universality class in the close-packed limit ($\varepsilon \rightarrow 0$). Nevertheless, for Manna model and directed percolation under $d < 4$, the Harris criterion ($d\nu_{\perp} > 2$) [41–44] is violated. This implies that disorder may have significant influence on the dynamic criticality. Therefore, a comprehensive and detailed study of the dynamic criticality of the BRO model in the high density regime is needed to fully resolve this issue.

In this work, we study two types of BRO model with or

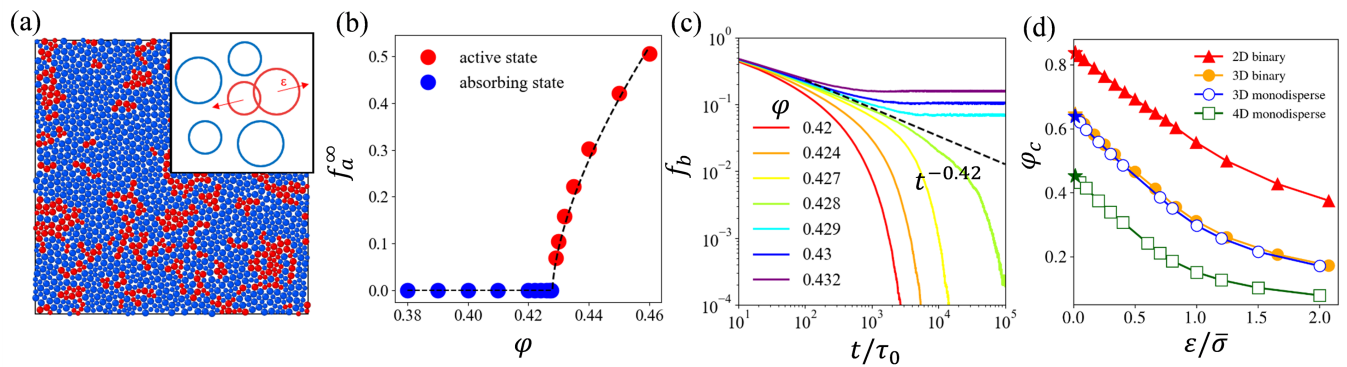


FIG. 1: (a) Schematic of conserved BRO model: overlapping particles (red) become active and take pairwise repulsive displacements. (b) Order parameter f_a^∞ as a function of packing fraction φ at $\varepsilon=2.0\sigma$. (c) Evolution of $f_b(t)$ for systems at $\varepsilon=2.0\sigma$ under various φ . The dashed line represents the power law $t^{-0.42}$. Here $N=65536$. (d) Critical packing fractions φ_c for 2D binary (red line), 3D binary (orange dots), 3D monodisperse (blue circles) and 4D monodisperse (green open squares) systems with conserved BRO dynamics at different ε . Here $\bar{\sigma}$ represents the average diameter of particles. Asterisks mark the extrapolated φ_c for $\varepsilon \rightarrow 0$, i.e., 0.838 (2D), 0.645 (3D binary), 0.640 (3D monodisperse) and 0.453 (4D), which are consistent with the RCP states [7, 10–13].

without center of mass conservation (CMC) [33, 34, 45] and find both of them exhibit anomalous critical behaviors at high density, which deviate from the Manna universality class. In 3D monodisperse sphere systems, we find that the absorbing transition is interrupted by crystallization. In binary mixture systems without crystallization, an unreported universality class of dynamic phase transition, i.e., absorbing to active-glass transition, is identified, which is characterized by critical exponents different from the Manna universality class. With further increase of the critical density by decreasing ε , dynamic heterogeneity and Griffiths effects emerge, which smooth the dynamic transition and broaden the critical point into a pseudo-critical regime. As $\varepsilon \rightarrow 0$, the dynamic transition becomes equivalent to heterogeneous directed percolation (DP) due to particle immobility set by the jamming. These results indicate that while the BRO models can generate RCP configurations, the criticality of the transition is fundamentally reshaped by the RCP state. This discourages a direct mapping of the jamming transition to an absorbing phase transition for disordered systems under $d \leq 4$. For closed-packed crystal structures, the Griffiths effect is absent. The dynamic criticality is thus restored, but still deviates from the Manna universality class. We propose a field theory with fractional time dynamics which can unify the above phenomena in the same framework, revealing a complicated interplay between dynamic criticality and spatial annealed/quenched disorder. Our findings can be a starting point to study the dynamic criticality of more complicated disordered systems, like the learning process of artificial neural networks [35, 39, 46].

MODEL AND SIMULATIONS

In BRO models, particles are first randomly distributed in the space of dimension d . In each discrete time step, if a particle is isolated without overlapping with other particles, it is considered inactive and remains stationary. On the contrary, if two particles overlap, they are considered as active and a pair of repulsive central displacements with opposite directions are assigned to each other, as shown in Fig. 1(a) [33–35, 45, 47]. In this work, we explicitly consider two types of BRO dynamics, classified by whether they conserve the center of mass of the system [45]. In the conserved dynamics, the displacements of a pair of overlapped particles have the same magnitude randomly chosen from a uniform range of $[0, \varepsilon/2]$. If a particle overlaps with multiple particles, these displacements (vectors) are superimposed [45, 47]. In the non-conserved dynamics, the displacement magnitude of each overlapped particle is randomly chosen from $[0, \varepsilon/2]$, and the direction of displacement of the particle is from the mass center of overlapped clusters to the center of this particle [33, 34]. Since the two types of BRO model exhibit similar results, in the main text, we mainly show the results of conserved BRO model, while leaving the data of non-conserved one in Supplementary Information (SI).

We simulate N spherical particles in a hypercubic box of length L with periodic boundary conditions at packing fraction φ . Both monodisperse particle systems and equal-number binary mixtures of small and large particles are considered. In the latter, the particle diameter ratio is $\sigma_M/\sigma_m = 1:\sqrt{2}$. The small particle diameter in each system is chosen as the unit length σ and τ_0 is the unit time.

To study the dynamic criticality of the system, we analyze the ensemble of dynamic trials starting from random

configurations. We define the survival activity of the system at time t

$$f_a(\tau, t) = \frac{\langle N_a(\tau, t) \rangle_a}{N} \quad (1)$$

where $N_a(t)$ is the number of active particles at time step t . Here, $\tau = (\varphi - \varphi_c)/\varphi_c$ is the distance to the critical point. Note that $\langle \cdot \rangle_a$ here indicates that the average is only on trials that remain active up to time t . Generally, below the critical point ($\tau < 0$), the system falls into an absorbing phase with $f_a^\infty \equiv f_a(t \rightarrow \infty) = 0$, while above the critical point ($\tau > 0$), the system stays in an active state with $f_a^\infty > 0$ (see Fig. 1(b)). At the critical point ($\tau = 0$), $f_a(t)$ is expected to decay following a power law $t^{-\alpha}$.

We can further define the overall activity of the system averaged over all trials

$$f_b(\tau, t) = \frac{\langle N_a(t) \rangle}{N} = f_a(\tau, t)P_s(\tau, t) \quad (2)$$

where $P_s(\tau, t)$ is the survival probability of the active phase up to time t , which can be used to define the characteristic life time t^* of the trials. At the critical point, $f_b(t)$ should also decay following a power law $t^{-\alpha}$. Below and above the critical point, $f_b(t)$ deviates from the power law (see Fig. 1(c)). As shown later, $f_b(t)$ provides a good measure of the Griffiths effects. Details about the finite-size scaling of $f_a(\tau, t)$, $f_b(\tau, t)$, $P_s(\tau, t)$ and $t^*(\tau)$, the definition of critical exponents and other quantities can be found in the Methods Section.

RESULTS

Anomalous critical behaviors at high density

Based on the finite-size scaling analysis, we can determine the critical packing fraction φ_c of systems under different ε , which are summarized in Fig. 1(d). By extrapolating these data to $\varepsilon \rightarrow 0$, we obtain $\varphi_c = 0.838$ in 2D, $\varphi_c = 0.645$ in 3D binary, $\varphi_c = 0.640$ in 3D monodisperse, $\varphi_c = 0.453$ in 4D for both monodisperse and binary systems. Similar data for non-conserved BRO model can be found in Fig. S1. These values are consistent with the reported RCP packing fractions φ_{RCP} [7, 10–13], and in line with previous studies [33, 34].

Nevertheless, for 3D monodisperse conserved BRO model under $0.2\sigma < \varepsilon < 0.7\sigma$, we find that the dynamic transition does not exhibit standard critical phenomena (Fig. 2(a)). Detailed structural analysis based on classical crystal order parameter (see SI) reveals that the dynamic transition is disrupted by crystallization (Fig. 2(b)). For non-conserved BRO model, crystallization is also observed when $0.2\sigma < \varepsilon < 0.5\sigma$ (See Fig. S2). This forces us to focus on binary system, where crystallization is avoided. However, we find that the critical

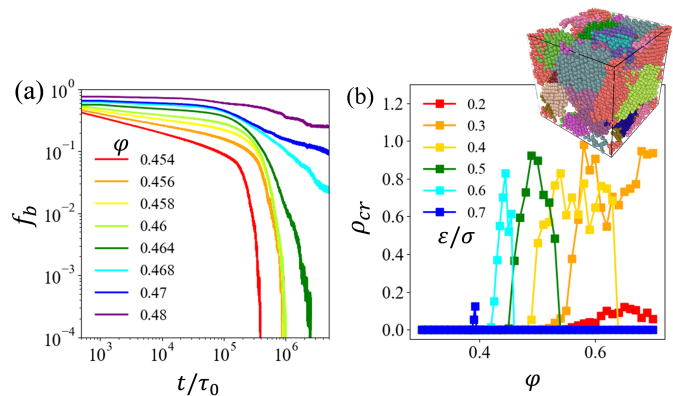


FIG. 2: (a) The evolution of the activity $f_b(t)$ at different packing fractions at $\varepsilon = 0.5\sigma$. (b) The particle fraction in crystal phase ρ_{cr} under different ε and packing fractions at $t = 10^6\tau_0$. Inset: The crystallization in a 3D monodisperse system under conserved BRO dynamic with $\varepsilon = 0.5\sigma$ at packing fraction $\varphi = 0.480$ and $t = 10^6\tau_0$. Different colors represent different crystal grains.

behaviors of binary systems still mismatch the Manna universality class.

In Fig. 3(a-d), we show the finite-size scaling of $f_a(t)$, $P_s(t)$, $f_a^\infty(\tau)$ and $t^*(\tau)$ for 2D binary systems with $\varepsilon = 0.8\sigma$ at $\varphi_c = 0.6496$. The obtained critical exponents β , ν_{\parallel} , α , z^* and ν_{\perp} as functions of ε are shown in Fig. 3(e-h). For $\varepsilon > 1.0\sigma$ (Regime I, cyan), these critical exponents are consistent with the Manna universality class. When $0.3\sigma < \varepsilon < 1.0\sigma$ (Regime II, orange), we find non-monotonic behaviors of ν_{\perp} , α , and z , inconsistent with the Manna universality class. Further decreasing ε below 0.3σ (Regime III, red), the failure of standard finite size scaling and the uncertainty of the critical point are observed (In Fig. S3-S5). In Fig. S6-10, we also present the exponents measured in three and four dimensional systems for both conserved and non-conserved BRO systems. We find that the general behavior of the critical exponents and finite size scaling remains qualitatively the same. This indicates that the anomalous criticality of the BRO model is robust at high density, insensitive to the dimensionality, particle ratio and CMC.

Absorbing to active-glass transition In Regime I, the step size ε is larger than the particle size. Thus, the motion of active particles is not constrained by neighbouring particles. Thus, the mean-square-displacement (MSD) of active particles shows diffusion scaling as shown in Fig. 4(a). Here, the solid and open symbols represent systems above and below the critical point, respectively. The diffusion scaling in sub-critical systems indicates that the absorbing transition is essentially a non-local searching process for a non-overlapping configuration, a characteristic of the Manna universality class [50, 51].

As ε decreases, φ_c increases. Due to the repulsive displacement in the BRO model, the particles are caged by

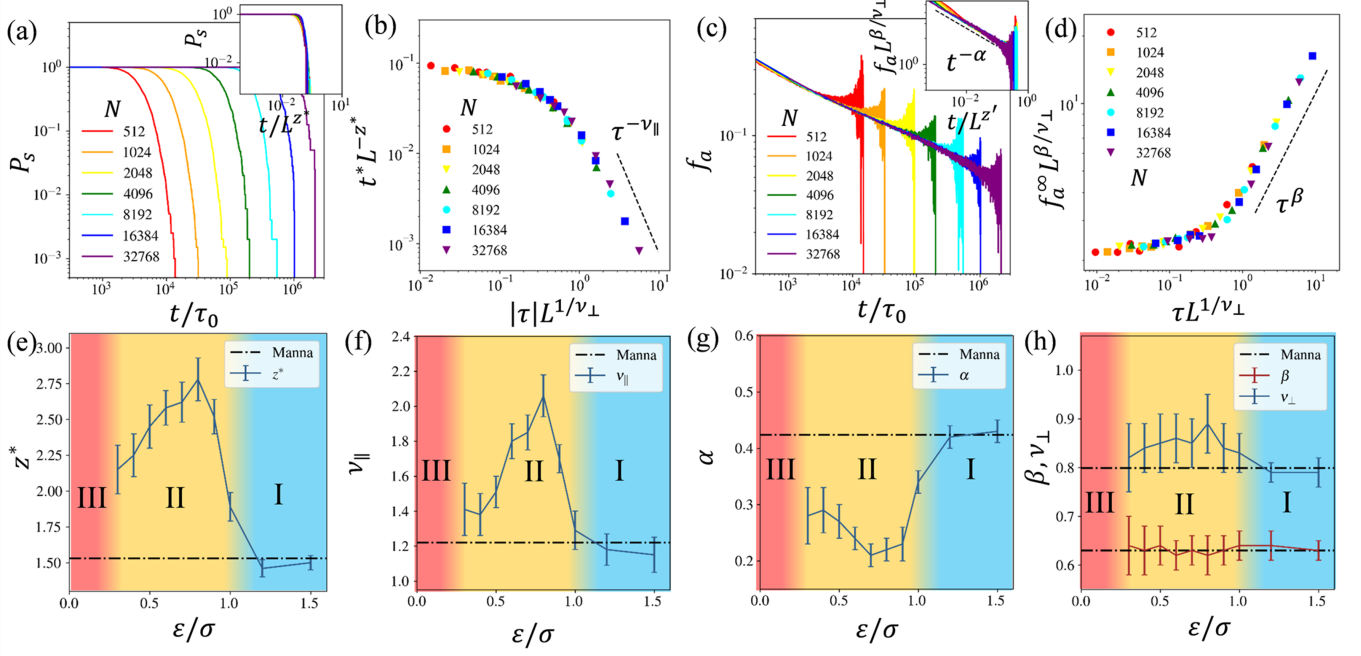


FIG. 3: (a, c) Finite size scaling for survival probability $P_s(t)$ and survival activity $f_a(t)$ at $\varepsilon=0.8\sigma$, $\varphi_c=0.6496$. (b, d) Finite size scaling for t^* and f_a^∞ at $\varepsilon=0.8\sigma$. (e, f, g, h) Critical exponents of z^* , ν_{\parallel} , α , β and ν_{\perp} as functions of ε , from which one can distinguish three regimes (from right to left): regime I (light blue), regime II (light orange), regime III (light red). The dotted lines represent the values of z^* , ν_{\parallel} , α , β and ν_{\perp} in the Manna universality class [48, 49].

their neighbours. This effect is shown in Fig. 4(c) for systems with $\varepsilon=0.5\sigma$, where one can find an early-time plateau or sub-diffusion regime in MSD for systems above the critical point, a characteristic of the glass-forming liquids [52–55]. In Fig. 4(b), we plot the measured diffusion coefficient D of active particles and f_a^∞ as a function of φ under different ε . We can clearly distinguish active states with D as low as $10^{-6}\sigma^2/\tau_0$ for $\varepsilon<\sigma$. The decoupling between f_a^∞ and D suggests that in Regime II, the absorbing phase transition is essentially an absorbing to active-glass transition, where particles can only find a non-overlapping absorbing configuration through local arrangements instead of non-local searching. Interestingly, when φ further increases, the system with $\varepsilon<1.0\sigma$ becomes diffusive again, which corresponds to the yielding transition of granular systems under oscillatory shearing [20, 23, 25–27]. In Fig. 4(d), we summarize the dynamic behaviors of the system in a phase diagram, where the active-glass phase can be clearly identified in the cyan regime. The non-conserved BRO model also has a similar phase diagram (see Fig. S11).

The fundamental difference between absorbing to active-glass transition and the Manna universality class can be distinguished by field theory. It is known that the Manna universality class is described by a non-conserved field $\rho(\mathbf{r}, t)$ (active particle density field) coupling with a non-diffusive conserved field $\psi(\mathbf{r}, t)$ (total

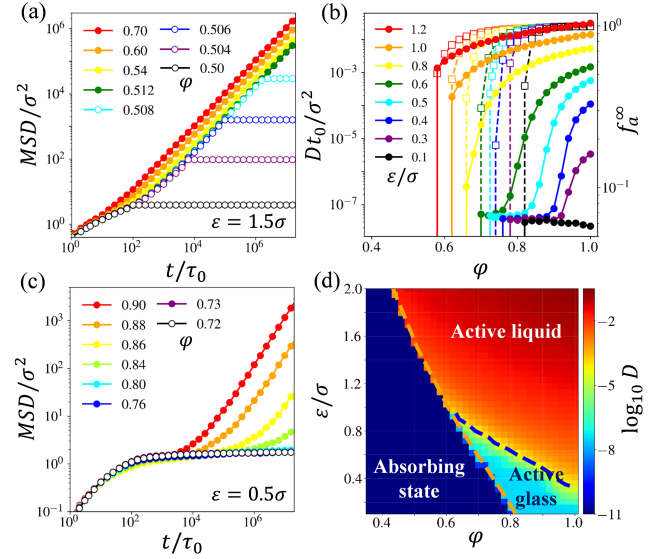


FIG. 4: (a, c) MSD(t) for systems under different ε , where the open/solid symbols represent the absorbing/active state, respectively. (b) Diffusion coefficients D (solid line) and f_a^∞ (dotted line) as functions of φ at various ε . (d) Dynamic phase diagram of the system in the dimensions of packing fraction φ and ε . The yellow line is the absorbing-active transition line. The blue line indicates the ‘yielding transition’ line (cyan regime).

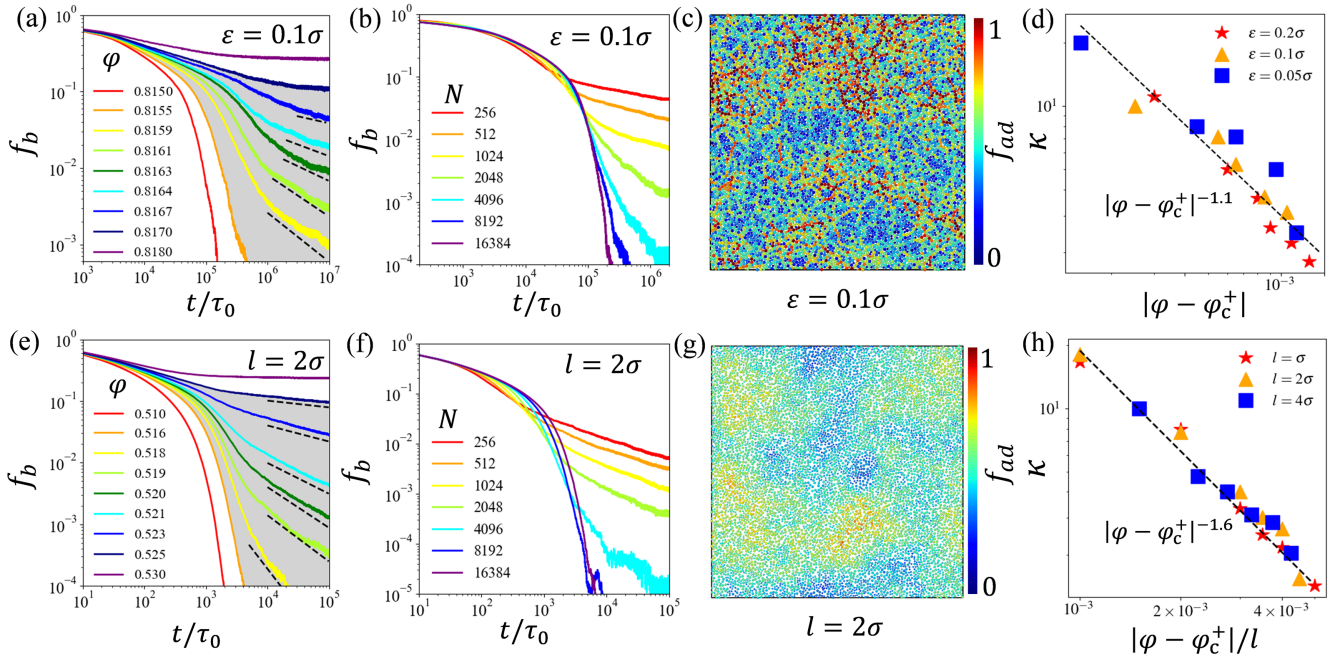


FIG. 5: Griffiths effects for original BRO model with $\varepsilon=0.1\sigma$ (upper row) and modified BRO models with quenched-disorder ($\varepsilon=1.5\sigma$, $\Delta\varepsilon=1.2\sigma$) (lower row). (a, e) Evolution of $f_b(t)$ at different φ , where Griffiths regimes are painted in gray. Here, $N=8192$. (b, f) Evolution of $f_b(t)$ at different N . Here, $\varphi=0.8152$ (upper) and 0.5160 (lower). (c, g) Distributions of normalized activity duration f_{ad} for systems studied in (b, f) with $N=8192$. (d, h) Measured κ index (Eq.(5)) as a function of φ under different ε and l . In (d), $\varphi_c^+ = 0.7916, 0.8170, 0.8297$ for $\varepsilon=0.2, 0.1, 0.05\sigma$, respectively. In (h), $\varphi_c^+ = 0.526, 0.527, 0.531$ for $l=1, 2, 4\sigma$, respectively.

density field) [56, 57], namely,

$$\frac{\partial \rho(t)}{\partial t} = D\nabla^2 \rho + a\rho - b\rho^2 + w\rho\psi + \sigma_n \sqrt{\rho} \xi(t) \quad (3)$$

$$\frac{\partial^\theta \psi(t)}{\partial t^\theta} = D'\nabla^2 \rho, \quad (4)$$

with $\theta=1$. Note that a, b, w are fixed parameters determining the critical point [57]. The last term in Eq.(3) is the multiplicative noise term accounting for absorbing state transition. In the active-glass state, however, the dynamics of the $\psi(t)$ field in Eq.(4) is sub-diffusive due to the caging effect. This effect causes long-range temporal correlation, which can be phenomenologically described by fractional time derivative with $0 < \theta < 1$ [58–63], while the activity field is still diffusive as activity can spread by particle contact. Note that in principle one can also construct more sophisticated theories based on the mode-coupling theory [64, 65] to describe the glassy evolution of $\psi(t)$. Nevertheless, the fractional time description gives a more intuitive picture of how the caging effect changes the coupling between $\psi(t)$ and $\rho(t)$ fields, thus modifies the criticality of the Manna universality class. Further theoretical explorations are needed to confirm whether this simplification preserves all relevant factors near the critical point.

Griffiths effects in pre-jamming state When ε is further reduced below 0.3σ (Regime III), the critical

density of the system would approach that of RCP state. In this regime, caging-breaking events become unlikely and the topology of particle network remains unchanged in the activation process. We refer to this state as the pre-jamming state. Different from the conventional absorbing state transition, we find $f_b(t)$ in this state relaxes according to a continuous power law

$$f_b(t) \sim t^{-d/\kappa} \quad (5)$$

with the φ -dependent index [42]

$$\kappa \sim |\varphi - \varphi_c^+|^{-h} \quad (6)$$

in a wide density range $\varphi_c^- < \varphi < \varphi_c^+$, as shown in Fig. 5(a) and Fig. S12. Here h is an exponent on the ‘dirty’ critical point φ_c^+ [42]. Non-conserved BRO model under high density also exhibits a similar phenomenon (Fig. S15). The existence of this critical-like regime rather than critical point, is strong evidence of the Griffiths effects which is usually caused by spatial heterogeneity [42, 43, 66–69]. This effect becomes more pronounced with decreasing ε as shown in Fig. S12. In Fig. 5(h), we plot the measured κ as a function of $|\varphi - \varphi_c^+|$. The fitting gives $h=1.1$.

In the Griffiths phase, the quenched disorder generates strong dynamic heterogeneity in the relaxation process, characterized by quasi-static network composed of frequently overlapping particles. This can be visualized by the spatial distribution of normalized activity duration

f_{ad} , i.e., the fraction of time that a particle stays in an active state relative to twice of the average active duration of the whole system (See the SI for details). In Fig. 5(c), we show these distributions for systems with $\varepsilon=0.1\sigma$. One can observe non-uniform network structures of activity, resembling the dynamic heterogeneity of supercooled liquids or the force chain of the jammed state [70–73]. In Regime II, one can also find relatively weak dynamic heterogeneity, which would be smoothed out by further increasing ε to Regime I (Fig. S13).

In the Griffiths phase, the finite-size effect of $f_b(t)$ and $P_s(t)$ near criticality is also reversed, i.e., at the same density near the transition, small systems stay longer in the active state than large systems. This is best shown in Fig. 5(b) and Fig. 6(a). This abnormality is nevertheless consistent with the fact that small systems are more likely to be jammed near the jamming point [74, 75]. This suggests that close-packing significantly influences the criticality of absorbing phase transition in this regime.

To further prove that the above phenomena are results of the Griffiths effects, we manually add quenched disorder in systems located at Regime I, by making ε spatially dependent. More explicitly, the system is divided into cells of size l . Each cell (i, j) has its own $\varepsilon_{i, j}$ set as

$$\tilde{\varepsilon}_{i, j} = \varepsilon + \Delta\varepsilon \xi_{i, j} \quad (7)$$

where $\Delta\varepsilon$ is the strength of the quenched disorder and $\xi_{i, j}$ is a spatially-uncorrelated random number uniformly distributed within $(-1, 1)$. Thus for $\Delta\varepsilon=0$, we return to the original BRO model. In Fig. 5(e, g), we show $f_b(t)$ and the activity duration distribution for systems under $\varepsilon=1.5\sigma$ and $\Delta\varepsilon=1.2\sigma$. Compared with $\Delta\varepsilon=0$ cases that exhibit standard critical behaviors, the introduction of $\Delta\varepsilon$ induces obvious dynamic heterogeneity and the Griffiths effects similar to Fig. 5(a, c). In Fig. 5(f, h), we plot the finite-size scaling of $f_b(t)$ and $\kappa(|\varphi - \varphi_c^+|)$ for these systems, which exhibits strong similarity with high density systems shown in Fig. 5(b, d). Moreover, we find that the effect of increasing l (correlation length of quenched disorder) is similar to decreasing ε in pre-jamming states (Fig. S12, Fig. S13). This indicates that the correlation length diverges in the BRO model as $\varepsilon \rightarrow 0$, in accordance with what happens at the jamming transition point [76]. Nevertheless, this mapping fails in the close-packed limit when the correlation spans the system.

Mapping to heterogeneous DP Finally, we study the critical behaviors of the BRO model in the close packed limit ($\varepsilon \rightarrow 0$). In this limit, the particle configuration can be regarded as static during the relaxation process (corresponding to $\theta \rightarrow 0$ in Eq. (4)). Although the spatial fluctuation of ψ field is small, it acts as strong quenched disorder influencing the dynamics of $\rho(t)$, as the coupling coefficient ω diverges in the close-packed limit.

More explicitly, the fluctuation of density field around

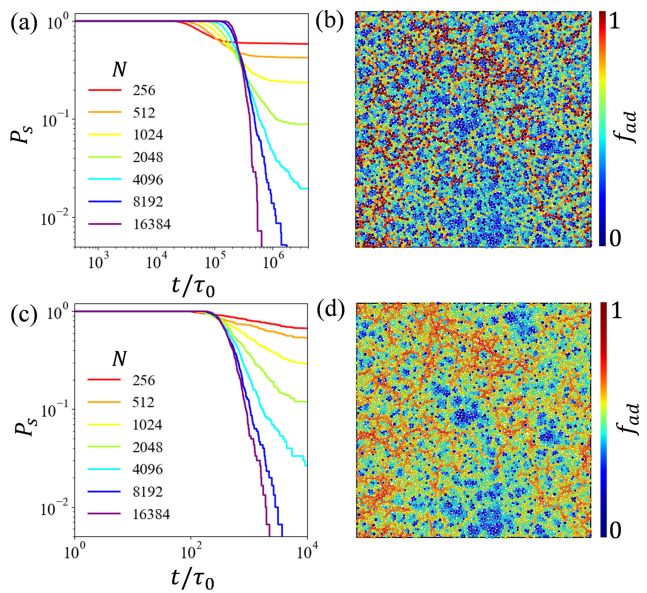


FIG. 6: (a, c) Finite size effects of survival probability of dynamic trajectory $P_s(t)$. (b, d) Distributions of normalized activity duration. (a, b) are for the original BRO models near the transition point at $\varepsilon=0.01\sigma$ and $\varphi=0.8380$. (c, d) are for the heterogeneous contact model at $P_e=0.780$ and $k=1$ based on the same configuration as in (b).

mean value ψ_0 can be decomposed into plastic contribution $\delta\psi_p(t)$ and elastic contribution $\delta\psi_e(t)$ [77, 78], i.e.,

$$\delta\psi(t) = \delta\psi_p(t) + \delta\psi_e(t) \quad (8)$$

where $\delta\psi_p(t)$ is caused by the rearrangement of the topological networks of particles due to cage-breaking relaxation, while $\psi_e(t)$ is attributed to vibrational displacements of particles in the cage, whose magnitude can be reflected by Debye-Waller factor [78]. For disordered systems near jamming point, $\psi_p(t)$ freezes and hardly evolves, becoming a spatial quenched disorder $\delta\psi_{qc}$ whose influence is persistent and much stronger than the fluctuating $\delta\psi_e(t)$. By neglecting $\delta\psi_e(t)$ field, Eqs. (3-4) reduce to the field theory of directed percolation (DP) with quenched disorder, or heterogeneous DP [42, 67, 69].

$$\frac{\partial\rho(t)}{\partial t} = D\nabla^2\rho + a'\rho - b\rho^2 + \omega\rho\delta\psi_{qc} + \sigma_n\sqrt{\rho}\xi(t) \quad (9)$$

where $a' = a + \omega\psi_0$. The classical contact model on a hierarchical heterogeneous network is the simplest realization of heterogeneous DP [44, 79, 80]. To test the above idea, we simulate a contact model on the networks composed of nearly jammed particles generated by the BRO model at $\varepsilon=0.01\sigma$, where each particle represents a node. We find that the topology of the contact network alone does not affect the critical behaviors of systems. However, if the infection rate of a node is proportional to the activity durations of the corresponding particle, i.e., $k=1$ (see the Method Section for details), the activity

ε	α	ν_{\perp}	ν_{\parallel}	β	z^*	z
0.01σ	0.64(4)	0.79(2)	0.84(4)	0.64(2)	1.43(8)	1.06(8)
0.2σ	0.64(5)	0.80(2)	0.82(5)	0.63(3)	1.44(8)	1.02(9)
Manna	0.419	0.799	1.225	0.639	1.533	1.533

TABLE I: Critical exponents measured in 2D crystal systems under conserved BRO dynamics. Reference values of the Manna universality class are from Ref. [48, 49].

duration distribution of this contact model exhibits dynamic heterogeneity resembling that of the high density BRO model (Fig. 6(b, d)). Correspondingly, the finite size scaling of $P_s(t)$ in Fig. 6(c) also exhibits similar anomalous behaviors as the BRO model in the close packing limit (Fig. 6(a)). Moreover, the Griffiths effects become stronger as the heterogeneity increases in the DP model, i.e., for $k=2, 4$. (see Fig. S14). These similarities prove that the BRO model in the nearly jammed configuration corresponds to heterogeneous DP model.

Dynamic criticality in crystal phase In a previous study, the absorbing transition of conserved BRO model in crystal phase has also been suggested to reside in the Manna universality [47]. We analyse this issue within the above theoretical framework. For crystal structures without defects, the quenched disorder disappears, i.e., $\delta\psi_p(t)=0$. Thus Griffiths effect is absent and the fluctuation of $\psi(t)$ is solely determined by $\delta\psi_e(t)$ which is connected to local strain (displacement) field $\mathbf{u}(t)$, i.e., $\psi_e(t)=\psi_0\nabla\mathbf{u}(t)$ [81]. The particle velocity field is $\mathbf{v}(t)=\partial\mathbf{u}(t)/\partial t$. This gives the field equation for critical dynamics of crystal phase

$$\begin{aligned} \frac{\partial\rho(t)}{\partial t} &= D\nabla^2\rho + a\rho - b\rho^2 + \omega\rho\delta\psi_e(t) + \sigma_n\sqrt{\rho}\xi(t) \quad (10) \\ \frac{\partial\delta\psi_e(t)}{\partial t} &= \psi_0\nabla\mathbf{v}(t), \quad (11) \end{aligned}$$

In isotropic systems, $\mathbf{v}(t)=\Gamma\nabla p(t)$ where $p(t)$ is the effective pressure. Near the critical point, $p(t)$ should be proportional to $\rho(t)$ as a first order approximation, which gives $\mathbf{v}(t)\sim\nabla\rho(t)$ [56, 57]. Then Eq. (10-11) returns to the field equation for the Manna universality class. However, the intrinsic anisotropy of crystal structures does not guarantee this reduction. In Table I and Fig. S16, we give the measured critical exponents for crystal phase. We find notable deviations from the Manna universality class for dynamic critical exponents α , ν_{\parallel} and z . The difference between our results and Ref. [47] might be that Ref. [47] did not use defectless crystal structures as initial configurations.

Long wavelength density fluctuations Finally, we discuss the density fluctuation of the system. It is

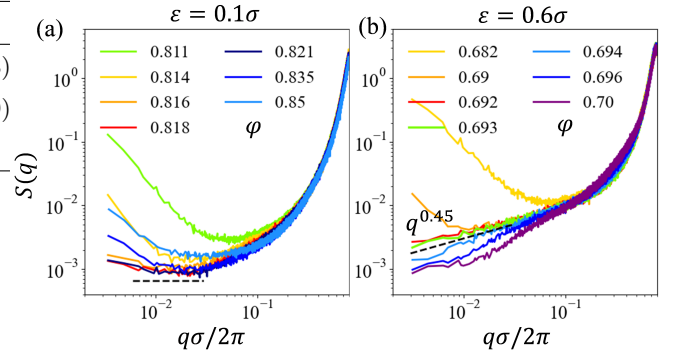


FIG. 7: Structure factor for 2D conserved binary BRO systems. For (b), $\varphi_c=0.693$.

known that at the critical point of RO/BRO model at large ε , the density fluctuation is suppressed, giving rise to the critical hyperuniform state with structure factor $S(q)\sim q^{0.45}$ (2D) and $S(q)\sim q^{0.25}$ (3D) [31, 32]. This critical hyperuniform state is a dynamic state accompanied by the intermittent diffusion of active particles. It was argued that this hyperuniform scaling remains unchanged when the system approaches the jammed point $\varepsilon\rightarrow 0$ [33, 34]. Nevertheless, the exponent 0.25 for 3D system is too small to be accurately determined near the jamming point (Fig. S18). For 2D conserved binary BRO model, we find similar hyperuniformity scaling $S(q)\sim q^{0.45}$ when $\varepsilon=0.6\sigma$ (Fig. 7(b)), consistent with Ref. [33]. However, by further decreasing ε to 0.1σ , an obvious deviation of $S(q)$ from $q^{0.45}$ can be found (Fig. 7(a)). Similar behaviors can also be found in non-conserved BRO model in Fig. S17. This indicates that $S(q)$ at jamming point is controlled by the contact network of jamming configuration, rather than the critical dynamics of the Manna universality class.

DISCUSSION AND CONCLUSION

In the above analysis, we only discuss the conserved BRO model. Actually, the non-conserved BRO model exhibits qualitatively the same results (Fig. S1, S2, S6, S8, S10, S11, S15, S17, Table SI). Quantitatively, the non-conserved BRO model introduces additional randomness compared with the conserved BRO model. Thus the caging-effect is relatively weaker and the active glass phase area is smaller than that of the conserved BRO model (Fig. S11).

In summary, we investigate the critical behavior of two types of BRO model in dense monodisperse and binary systems in $d=2$ to 4. We find that anomalous critical phenomena emerge as the critical density increases by decreasing displacement size ε . For 3D monodisperse systems at intermediate critical density, the crystallization interrupts the dynamic phase transition. For binary sys-

tems at intermediate critical density, the measured critical exponents deviate from the Manna universality class due to the caging effects, signifying the existence of a new universality class of dynamic phase transition, i.e., the absorbing to active glass transition. For disordered systems at higher density, the quenched disorder of contact networks triggers the pronounced Griffiths effects, smearing out the dynamic critical point. In the $\varepsilon \rightarrow 0$ limit, the BRO model becomes equivalent to DP on a heterogeneous network. Our results demonstrate that although the BRO model can generate RCP configurations, the criticality of the dynamic transition is fundamentally reshaped by the geometric rigidity of the RCP state. These findings discourage previous attempts to directly associate the jamming transition in disordered systems with the Manna universality class under $d \leq 4$. For close-packed crystal phase, the Griffiths effect is absent, but we find that the dynamic criticality still deviates from the Manna universality class due to the anisotropy of the crystal structures. We propose a field theory with fractional time dynamics which unifies the above complicated dynamic behaviors, revealing a deep connection between dynamic criticality, spatial annealed/quenched disorder and jamming. Our work could potentially be related to ultra-stable glass and the Gardner transition [39, 82–85], and enriches the studies of the dynamic criticality of more complicated artificial neural networks [39, 46], like the learning process of spherical negative perceptron model [35].

METHOD

Finite-size scaling of absorbing phase transition For typical second-order absorbing phase transitions, $f_a(t)$ should satisfy the finite-size scaling relationship [49, 86–88]

$$f_a(t, \tau, L) \propto L^{-\beta/\nu_\perp} \mathcal{F}(tL^{-z'}, \tau L^{1/\nu_\perp}) \quad (12)$$

where $\mathcal{F}(x, y)$ is the scaling function satisfying $\mathcal{F}(x, 0) \sim x^{-\alpha}$ for $x \ll 1$ and $\mathcal{F}(x, 0) \sim \text{const.}$ for $x \gg 1$. In a fully active state, the decay of $f_a(t, 0, L)$ is independent of L at an earlier stage, which leads to $z' = \beta/(\nu_\perp \alpha)$. On the other hand, f_a^∞ satisfies

$$f_a^\infty(\tau, L) \propto L^{-\beta/\nu_\perp} \mathcal{F}(\infty, \tau L^{1/\nu_\perp}) \quad (13)$$

where $\mathcal{F}(\infty, y) \sim y^\beta$ for $y \gg 1$ and $\mathcal{F}(\infty, y) \sim \text{const.}$ for $y \ll 1$. Furthermore, the survival probability $P_s(\tau, t)$ of the active phase up to time t should satisfy

$$P_s(t, \tau, L) \propto \mathcal{P}(tL^{-z^*}, \tau L^{1/\nu_\perp}) \quad (14)$$

where $\mathcal{P}(x, 0) \sim 1$ for $x \ll 1$ and $\mathcal{P}(x, 0) \rightarrow 0$ for $x \gg 1$. From Eq. (14), we can also obtain the finite size scaling relationship for the characteristic time of the activity

decay t^* satisfying $\mathcal{P}(t^*L^{-z^*}, \tau L^{1/\nu_\perp}) = 0.5$, i.e.,

$$t^* \propto L^{z^*} \mathcal{T}(\tau L^{1/\nu_\perp}) \quad (15)$$

where $\mathcal{T}(x) \sim \text{const.}$ for $x \ll 1$ and $\mathcal{T}(x) \rightarrow x^{-\nu_\parallel}$ for $x \gg 1$. By definition, $z = \nu_\parallel/\nu_\perp$ is the dynamic critical exponent. For a typical absorbing phase transition, one should expect $z = z' = z^*$.

Heterogeneous contact model In the classical contact model, two important controlling parameters are the basic infection rate P_e and recovery rate P_r [49, 79, 80]. The probability that the healthy site i becomes infected by an adjacent infected site in the next time step is

$$P_{e,i} = P_e \frac{n_a(i)}{n_{neib}(i)} \quad (16)$$

where $n_a(i)$ represents the number of infected neighbors of the particle i , and $n_{neib}(i)$ is the total number of neighbors of the particle i . The recovery rate of each site, i.e., the probability that an infected site becomes healthy in the next time step, is $P_r = 1 - P_e$. We establish a contact network based on the particle configuration generated by BRO dynamics, where the positions of particles are the nodes of the network. A contact bond is assumed between the two nodes if their distance is less than 0.5σ . We introduce the heterogeneity by making the infection rate of site i coupling with the activity duration $f_{ad}(i)$ of the particle, i.e.,

$$P_{e,i} = f_{ad}(i)^k P_e \frac{n_a(i)}{n_{neib}(i)}. \quad (17)$$

Here $f_{ad}(i)$ is in the range of $(0, 1)$. As k increases, the heterogeneity becomes more prominent. We study different basic infection rate cases under $k=1, 2$ and 4 . We find that the Griffiths effects become stronger as k increases (see Fig. S14).

Acknowledgments: The authors are grateful to Ran Ni, Ning Xu, Hao Hu and Hua Tong for helpful discussions. This work is supported by the National Natural Science Foundation of China (No. 12347102, 12275127), the Natural Science Foundation of Jiangsu Province (No. BK20233001, No. BK20250058), the Fundamental and Interdisciplinary Disciplines Breakthrough Plan of the Ministry of Education of China (No. JYB2025XDXM502), Program for Innovative Talents and Entrepreneur in Jiangsu, the Fundamental Research Funds for the Central Universities (0204-14380249, KG202501), the Innovation Program for Quantum Science and Technology (No. 2024ZD0300101). The simulations are performed on the High-Performance Computing Center of Collaborative Innovation Center of Advanced Microstructures, the High-Performance Computing Center (HPCC) of Nanjing University.

* lql@nju.edu.cn

† myqiang@nju.edu.cn

- [1] V. Trappe, V. Prasad, L. Cipelletti, P. Segre, and D. A. Weitz, Jamming phase diagram for attractive particles, *Nature* **411**, 772 (2001).
- [2] A. J. Liu and S. R. Nagel, The jamming transition and the marginally jammed solid, *Annu. Rev. Condens. Matter Phys.* **1**, 347 (2010).
- [3] R. P. Behringer and B. Chakraborty, The physics of jamming for granular materials: a review, *Reports on Progress in Physics* **82**, 012601 (2018).
- [4] Y. Deng, D. Pan, and Y. Jin, Jamming is a first-order transition with quenched disorder in amorphous materials sheared by cyclic quasistatic deformations, *Nature Communications* **15**, 7072 (2024).
- [5] J. D. Bernal and J. Mason, Packing of spheres: coordination of randomly packed spheres, *Nature* **188**, 910 (1960).
- [6] G. D. Scott, Packing of spheres: packing of equal spheres, *Nature* **188**, 908 (1960).
- [7] J. G. Berryman, Random close packing of hard spheres and disks, *Phys. Rev. A* **27**, 1053 (1983).
- [8] S. Torquato, T. M. Truskett, and P. G. Debenedetti, Is random close packing of spheres well defined?, *Phys. Rev. Lett.* **84**, 2064 (2000).
- [9] T. Aste, M. Saadatfar, and T. J. Senden, Geometrical structure of disordered sphere packings, *Phys. Rev. E* **71**, 061302 (2005).
- [10] M. Danisch, Y. Jin, and H. A. Makse, Model of random packings of different size balls, *Phys. Rev. E* **81**, 051303 (2010).
- [11] C. Anzivino, M. Casiulis, T. Zhang, A. S. Moussa, S. Martiniani, and A. Zaccone, Estimating random close packing in polydisperse and bidisperse hard spheres via an equilibrium model of crowding, *The Journal of Chemical Physics* **158**, 044901 (2023).
- [12] L. E. Silbert, D. Ertas, G. S. Grest, T. C. Halsey, and D. Levine, Geometry of frictionless and frictional sphere packings, *Phys. Rev. E* **65**, 031304 (2002).
- [13] M. Skoge, A. Donev, F. H. Stillinger, and S. Torquato, Packing hyperspheres in high-dimensional euclidean spaces, *Phys. Rev. E* **74**, 041127 (2006).
- [14] A. Donev, S. Torquato, F. H. Stillinger, and R. Connelly, Jamming in hard sphere and disk packings, *Journal of Applied Physics* **95**, 989 (2004).
- [15] A. Donev, F. H. Stillinger, and S. Torquato, Unexpected density fluctuations in jammed disordered sphere packings, *Phys. Rev. Lett.* **95**, 090604 (2005).
- [16] D. Hexner, A. J. Liu, and S. R. Nagel, Two diverging length scales in the structure of jammed packings, *Phys. Rev. Lett.* **121**, 115501 (2018).
- [17] J. Shang, Y. Wang, D. Pan, Y. Jin, and J. Zhang, Jamming as a topological satisfiability transition with contact number hyperuniformity and criticality, arXiv preprint arXiv:2506.16474 [10.48550/arXiv.2506.16474](https://arxiv.org/abs/10.48550/arXiv.2506.16474) (2025).
- [18] D. J. Pine, J. P. Gollub, J. F. Brady, and A. M. Leshansky, Chaos and threshold for irreversibility in sheared suspensions, *Nature* **438**, 997 (2005).
- [19] L. Corte, P. M. Chaikin, J. P. Gollub, and D. J. Pine, Random organization in periodically driven systems, *Nature Physics* **4**, 420 (2008).
- [20] C. Reichhardt, I. Regev, K. Dahmen, S. Okuma, and C. J. O. Reichhardt, Reversible to irreversible transitions in periodic driven many-body systems and future directions for classical and quantum systems, *Physical Review Research* **5**, 021001 (2023).
- [21] C. F. Schreck, R. S. Hoy, M. D. Shattuck, and C. S. O'Hern, Particle-scale reversibility in athermal particulate media below jamming, *Phys. Rev. E* **88**, 052205 (2013).
- [22] L. Milz and M. Schmiedeberg, Connecting the random organization transition and jamming within a unifying model system, *Phys. Rev. E* **88**, 062308 (2013).
- [23] K. Hima Nagamanasa, S. Gokhale, A. Sood, and R. Ganapathy, Experimental signatures of a nonequilibrium phase transition governing the yielding of a soft glass, *Physical Review E* **89**, 062308 (2014).
- [24] I. Regev, T. Lookman, and C. Reichhardt, Onset of irreversibility and chaos in amorphous solids under periodic shear, *Phys. Rev. E* **88**, 062401 (2013).
- [25] I. Regev, J. Weber, C. Reichhardt, K. A. Dahmen, and T. Lookman, Reversibility and criticality in amorphous solids, *Nature communications* **6**, 8805 (2015).
- [26] T. Kawasaki and L. Berthier, Macroscopic yielding in jammed solids is accompanied by a nonequilibrium first-order transition in particle trajectories, *Phys. Rev. E* **94**, 022615 (2016).
- [27] K. Nagasawa, K. Miyazaki, and T. Kawasaki, Classification of the reversible-irreversible transitions in particle trajectories across the jamming transition point, *Soft matter* **15**, 7557 (2019).
- [28] D. Pan, Y. Wang, H. Yoshino, J. Zhang, and Y. Jin, A review on shear jamming, *Physics reports* **1038**, 1 (2023).
- [29] A. Ghosh, J. Radhakrishnan, P. M. Chaikin, D. Levine, and S. Ghosh, Coupled dynamical phase transitions in driven disk packings, *Physical Review Letters* **129**, 188002 (2022).
- [30] P. Das, H. Vinutha, and S. Sastry, Unified phase diagram of reversible-irreversible, jamming, and yielding transitions in cyclically sheared soft-sphere packings, *Proceedings of the National Academy of Sciences* **117**, 10203 (2020).
- [31] E. Tjhung and L. Berthier, Hyperuniform density fluctuations and diverging dynamic correlations in periodically driven colloidal suspensions, *Phys. Rev. Lett.* **114**, 148301 (2015).
- [32] D. Hexner and D. Levine, Hyperuniformity of critical absorbing states, *Phys. Rev. Lett.* **114**, 110602 (2015).
- [33] S. Wilken, R. E. Guerra, D. Levine, and P. M. Chaikin, Random close packing as a dynamical phase transition, *Phys. Rev. Lett.* **127**, 038002 (2021).
- [34] S. Wilken, A. Z. Guo, D. Levine, and P. M. Chaikin, Dynamical approach to the jamming problem, *Phys. Rev. Lett.* **131**, 238202 (2023).
- [35] G. Zhang and S. Martiniani, Absorbing state dynamics of stochastic gradient descent, [arXiv preprint arXiv:2411.11834](https://arxiv.org/abs/2411.11834) (2024).
- [36] G. I. Menon and S. Ramaswamy, Universality class of the reversible-irreversible transition in sheared suspensions, *Phys. Rev. E* **79**, 061108 (2009).
- [37] S. Torquato, Hyperuniform states of matter, *Physics Reports* **745**, 1 (2018).
- [38] Q.-L. Lei and R. Ni, Hydrodynamics of random-organizing hyperuniform fluids, *Proceedings of the National Academy of Sciences* **116**, 22983 (2019).

- [39] S. Anand, G. Zhang, and S. Martiniani, Emergent universal long-range structure in random-organizing systems, *Nature Communications* (2026).
- [40] C. Ness and M. E. Cates, Absorbing-state transitions in granular materials close to jamming, *Phys. Rev. Lett.* **124**, 088004 (2020).
- [41] A. B. Harris, Effect of random defects on the critical behaviour of ising models, *Journal of Physics C: Solid State Physics* **7**, 1671 (1974).
- [42] T. Vojta and M. Dickison, Critical behavior and griffiths effects in the disordered contact process, *Phys. Rev. E* **72**, 036126 (2005).
- [43] T. Vojta and M. Y. Lee, Nonequilibrium phase transition on a randomly diluted lattice, *Phys. Rev. Lett.* **96**, 035701 (2006).
- [44] T. Vojta, A. Farquhar, and J. Mast, Infinite-randomness critical point in the two-dimensional disordered contact process, *Physical Review E—Statistical, Nonlinear, and Soft Matter Physics* **79**, 011111 (2009).
- [45] D. Hexner and D. Levine, Noise, diffusion, and hyperuniformity, *Phys. Rev. Lett.* **118**, 020601 (2017).
- [46] S. Spigler, M. Geiger, S. d’Ascoli, L. Sagun, G. Biroli, and M. Wyart, A jamming transition from under-to over-parametrization affects loss landscape and generalization, arXiv preprint arXiv:1810.09665 10.48550/arXiv.1810.09665 (2018).
- [47] L. Galliano, M. E. Cates, and L. Berthier, Two-dimensional crystals far from equilibrium, *Phys. Rev. Lett.* **131**, 047101 (2023).
- [48] S. Lübeck, Universal scaling behavior of non-equilibrium phase transitions, *International Journal of Modern Physics B* **18**, 3977 (2004).
- [49] M. Henkel, H. Hinrichsen, and S. Lübeck, *Non-equilibrium phase transitions: Absorbing Phase Transitions*, Vol. 1 (Springer, 2008).
- [50] S. S. Manna, Two-state model of self-organized criticality, *Journal of Physics A: Mathematical and General* **24**, L363 (1991).
- [51] K. J. Wiese, Hyperuniformity in the manna model, conserved directed percolation and depinning, *Phys. Rev. Lett.* **133**, 067103 (2024).
- [52] P. G. Debenedetti and F. H. Stillinger, Supercooled liquids and the glass transition, *Nature* **410**, 259 (2001).
- [53] L. Berthier and G. Biroli, Theoretical perspective on the glass transition and amorphous materials, *Rev. Mod. Phys.* **83**, 587 (2011).
- [54] H. Tanaka, Structural origin of dynamic heterogeneity in supercooled liquids, *The Journal of Physical Chemistry B* **129**, 789 (2025).
- [55] H. Tanaka, T. Kawasaki, H. Shintani, and K. Watanabe, Critical-like behaviour of glass-forming liquids, *Nature materials* **9**, 324 (2010).
- [56] M. Rossi, R. Pastor-Satorras, and A. Vespignani, Universality class of absorbing phase transitions with a conserved field, *Physical review letters* **85**, 1803 (2000).
- [57] R. Pastor-Satorras and A. Vespignani, Field theory of absorbing phase transitions with a nondiffusive conserved field, *Physical Review E* **62**, R5875 (2000).
- [58] R. Metzler and J. Klafter, The random walk’s guide to anomalous diffusion: a fractional dynamics approach, *Physics reports* **339**, 1 (2000).
- [59] J.-P. Bouchaud, Weak ergodicity breaking and aging in disordered systems, *Journal de Physique I* **2**, 1705 (1992).
- [60] R. Hilfer, Experimental evidence for fractional time evolution in glass forming materials, *Chemical physics* **284**, 399 (2002).
- [61] G. Marty and O. Dauchot, Subdiffusion and cage effect in a sheared granular material, *Physical review letters* **94**, 015701 (2005).
- [62] E. R. Weeks and D. A. Weitz, Subdiffusion and the cage effect studied near the colloidal glass transition, *Chemical physics* **284**, 361 (2002).
- [63] B. Riechers, A. Das, E. Dufresne, P. M. Derlet, and R. Maaß, Intermittent cluster dynamics and temporal fractional diffusion in a bulk metallic glass, *Nature Communications* **15**, 6595 (2024).
- [64] D. R. Reichman and P. Charbonneau, Mode-coupling theory, *Journal of Statistical Mechanics: Theory and Experiment* **2005**, P05013 (2005).
- [65] W. Götze, The essentials of the mode-coupling theory for glassy dynamics, *Condensed Matter Physics* (1998).
- [66] M. A. Muñoz, R. Juhász, C. Castellano, and G. Ódor, Griffiths phases on complex networks, *Phys. Rev. Lett.* **105**, 128701 (2010).
- [67] A. G. Moreira and R. Dickman, Critical dynamics of the contact process with quenched disorder, *Phys. Rev. E* **54**, R3090 (1996).
- [68] I. Webman, D. Ben Avraham, A. Cohen, and S. Havlin, Dynamical phase transitions in a random environment, *Philosophical Magazine B* **77**, 1401 (1998).
- [69] J. Hooyberghs, F. Iglói, and C. Vanderzande, Absorbing state phase transitions with quenched disorder, *Phys. Rev. E* **69**, 066140 (2004).
- [70] Y. Nishikawa, A. Ikeda, and L. Berthier, Relaxation dynamics of non-brownian spheres below jamming: Y. nishikawa et al., *Journal of Statistical Physics* **182**, 37 (2021).
- [71] J. F. Peters, M. Muthuswamy, J. Wibowo, and A. Torde-sillas, Characterization of force chains in granular material, *Phys. Rev. E* **72**, 041307 (2005).
- [72] F. Radjai, M. Jean, J.-J. Moreau, and S. Roux, Force distributions in dense two-dimensional granular systems, *Phys. Rev. Lett.* **77**, 274 (1996).
- [73] T. S. Majmudar, M. Sperl, S. Luding, and R. P. Behringer, Jamming transition in granular systems, *Phys. Rev. Lett.* **98**, 058001 (2007).
- [74] C. P. Goodrich, A. J. Liu, and S. R. Nagel, Finite-size scaling at the jamming transition, *Phys. Rev. Lett.* **109**, 095704 (2012).
- [75] N. Xu, J. Blawdziewicz, and C. S. O’Hern, Random close packing revisited: Ways to pack frictionless disks, *Phys. Rev. E* **71**, 061306 (2005).
- [76] C. S. O’hern, L. E. Silbert, A. J. Liu, and S. R. Nagel, Jamming at zero temperature and zero applied stress: The epitome of disorder, *Physical Review E* **68**, 011306 (2003).
- [77] S. Torquato, G. Zhang, and F. H. Stillinger, Ensemble theory for stealthy hyperuniform disordered ground states, *Phys. Rev. X* **5**, 021020 (2015).
- [78] J. Kim and S. Torquato, Effect of imperfections on the hyperuniformity of many-body systems, *Phys. Rev. B* **97**, 054105 (2018).
- [79] T. E. Harris, Contact Interactions on a Lattice, *The Annals of Probability* **2**, 969 (1974).
- [80] I. Jensen, Critical behavior of the three-dimensional contact process, *Phys. Rev. A* **45**, R563 (1992).

- [81] P. M. Chaikin and T. C. Lubensky, *Principles of Condensed Matter Physics* (Cambridge University Press, Cambridge, 1995) pp. xx, 699.
- [82] Y. Wang, Z. Qian, H. Tong, and H. Tanaka, Hyperuniform disordered solids with crystal-like stability, *Nature Communications* **16**, 1398 (2025).
- [83] L. Berthier, P. Charbonneau, Y. Jin, G. Parisi, B. Seoane, and F. Zamponi, Growing timescales and lengthscales characterizing vibrations of amorphous solids, *Proceedings of the National Academy of Sciences* **113**, 8397 (2016).
- [84] P. Charbonneau, Y. Jin, G. Parisi, C. Rainone, B. Seoane, and F. Zamponi, Numerical detection of the gardner transition in a mean-field glass former, *Phys. Rev. E* **92**, 012316 (2015).
- [85] Q. Wang, D. Pan, and Y. Jin, Gardner transition coincides with the emergence of jamming scalings in hard spheres and disks, *arXiv preprint arXiv:2410.23797* (2024).
- [86] S. Lübeck and P. Heger, Universal finite-size scaling behavior and universal dynamical scaling behavior of absorbing phase transitions with a conserved field, *Physical Review E* **68**, 056102 (2003).
- [87] B. Zheng, Generalized dynamic scaling for critical relaxations, *Phys. Rev. Lett.* **77**, 679 (1996).
- [88] Q.-L. Lei, H. Hu, and R. Ni, Barrier-controlled nonequilibrium criticality in reactive particle systems, *Physical Review E* **103**, 052607 (2021).